

Robert Conzemius* and Evgeni Fedorovich
School of Meteorology, University of Oklahoma, Norman, Oklahoma

1. INTRODUCTION

Shear and buoyancy are both known to contribute to the development of boundary layers, whose characteristics include turbulent mixing of scalar quantities within the layer. Purely shear-driven boundary layers include airflow over an airplane wing and stream flow over a bottom surface. Buoyancy-driven boundary layers include the atmospheric convective boundary layer (CBL) and the upper levels of the ocean from the surface to the thermocline. If there is no mean flow (relative to the upper and lower limits of these layers), the CBL can be considered to be purely buoyancy-driven.

For the atmosphere, pure cases of buoyancy-driven and shear-driven boundary layers are difficult to find. In most situations, both shear and buoyancy are contributors to the growth and the internal structure of the boundary layer. Appropriate understanding of the combined effects of shear and buoyancy on boundary layer dynamics is necessary to best represent CBL effects in numerical weather prediction models.

This study explores the effects of wind shear on the growth and structure of the CBL and seeks to relate them within a general dynamical framework.

2. BACKGROUND

To date, investigations of the effects of wind shear on entrainment have concentrated on large eddy simulation (LES) and wind tunnel measurements. Sykes and Henn (1988) performed large eddy simulations of convective boundary layers with- and without wind shear and found that the transition from irregular polygonal structures characteristic of shear-free convection, to the roll structures found in sheared convection, occurred when the ratio of the convective velocity scale to the friction velocity was 0.35. Using LES, Moeng and Sullivan (1994) found a value of 0.65 for this ratio, and they also developed a conceptual model for velocity scaling and turbulence kinetic energy (TKE) budgets in a CBL, in which both shear and buoyancy effects were present. However, their model did not address the influence of shear in the entrainment zone on these budgets.

Brown (1996) used LES to evaluate the performance of two 1-D closure models used in forecasting models. These closure models were found to perform well for neutral boundary layers with or

without shear in the geostrophic wind. In sheared CBL cases, performance was not as good, but shear in the geostrophic wind did not seem to further degrade this performance. The simulations of Brown (1996) were for the non-entraining boundary layer only, and the effects of entrainment in sheared CBL regimes were not considered.

Fedorovich (1995) proposed an equation for the growth rate of sheared CBLs. The growth equation was obtained by integrating, over the depth of the CBL, the TKE balance equation derived from the assumptions of the zero-order jump (ZOJ) parameterization of the convective boundary layer. According to the equation, the velocity jump across the top of the CBL acts in a manner opposite to that of the temperature jump. Since stronger capping inversions slow the growth rate of the CBL, one might, therefore, expect enhanced boundary layer growth as shear across the entrainment zone is increased. In addition, shear effects should be more pronounced as buoyancy forcing is decreased relative to the amount of shear.

Finally, Fedorovich and Conzemius (2001) studied entrainment in heterogeneously stratified fluids without shear. Significant deviations from equilibrium entrainment occur when discontinuities in stratification are encountered by a growing CBL. These effects must be considered separately from those from shear alone but will likely play an important role in the results of this study.

3. METHODS

This study uses high-resolution LES to study the effects of shear on the CBL growth. The code is outlined in greater detail in Nieuwstadt and Brost (1986) and Wyngaard and Brost (1984). The model parameters are indicated in Table 1.

Table 1
LES Parameters

Minimum domain size	6.4x6.4x1.6 km
Minimum resolution	128x128x80 (20 m cells)
Bottom bound. cond.	Monin-Obukhov similarity
Top bound. cond.	Neumann (zero gradient)
Sponge layer	Top 20% of domain
Lateral bound. cond.	Periodic
Stratification	0.001 K/m to 0.010 K/m
Subgrid closure	Deardorff
Initial perturbation	2 K (temperature)
Initial CBL depth	0

Wind shear is implemented in the model in the form of a geostrophic balance term, in which speed is allowed to vary with height. The model atmosphere is not truly

* Corresponding author address: Robert Conzemius, School of Meteorology, University of Oklahoma, 100 East Boyd, Norman, OK 73019-1013; e-mail: bconzemi@rossby.metr.ou.edu

baroclinic, since a mean horizontal temperature gradient cannot be represented within the confines of periodic boundary conditions.

The large eddy simulations were divided into three basic classes: 1) shear-free CBL growth (geostrophic wind is zero throughout the model domain); 2) cases with a nonzero geostrophic wind, which does not vary with height; and 3) cases with shear in the geostrophic wind.

Statistics were calculated over horizontal planes in the model domain and averaged over 50 time steps. Statistics included first and second order moments in velocity, subgrid TKE, and temperature as well as third order moments of temperature and vertical velocity.

4. RESULTS

Results are focused on cases with a 0.010 K/m vertical virtual potential temperature gradient. These large-eddy simulations include a shear-free case (NS), a case with a constant 20 m/s geostrophic wind (G20), and a case with geostrophic wind increasing from zero at the surface to 20 m/s at $z=1.6$ km (GS).

4.1 CBL structure

Figure 1 shows the evolution of the profile of the u -component of the velocity during the LES runs G20 and GS cases. The latter case shows a rather substantial surface shear in the initial stages of the run. The surface shear decreases as the velocity jump across the CBL top increases. This feature makes G20 a good case for studying the effects of surface shear relative to those of entrainment zone shear on CBL structure and entrainment. The GS case exhibits a simultaneous increase in both the entrainment zone shear and the surface shear.

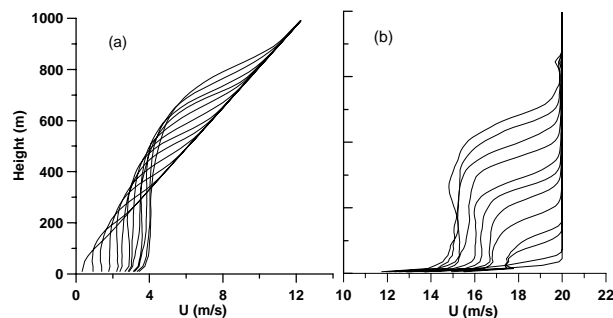


Figure 1. Profiles of the u -component of velocity: (a) GS case, and (b) G20 case.

Figure 2 presents horizontal distributions of the vertical velocity at $z=60$ m, after 8000 time steps into the (a) GS and (b) G20 simulations. The large surface shear in the G20 case immediately orients convective thermals and downdrafts into a horizontal convective roll pattern, and this pattern persists throughout the run. In the GS run, the surface shear never becomes as large as that in the G20 case, and thermals retain their irregular polygonal structure near the surface throughout the run.

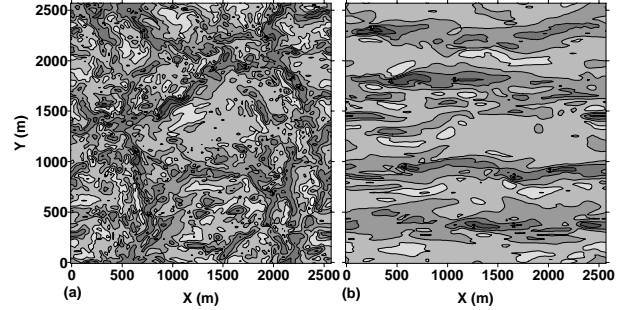


Figure 2. Vertical velocity at $z=60$ m after 8000 time steps: (a) GS case, (b) G20 case.

4.2 CBL growth rate

Results of the LES studies indicate that the effects of shear on the entrainment rate are dependent on the definition of boundary layer depth, z_r . Probably the most conventional definition of boundary layer depth is the level of the minimum in heat (or buoyancy) flux within the entrainment zone. If this level is taken as the CBL top, the CBL growth (entrainment) rate appears unaffected by the presence of wind shear. Figure 3 shows CBL depth versus time for the NS, G20, and GS cases. In all three cases, the growth rate closely follows the one half power law predicted using the assumptions of the ZOJ model of the atmospheric CBL.

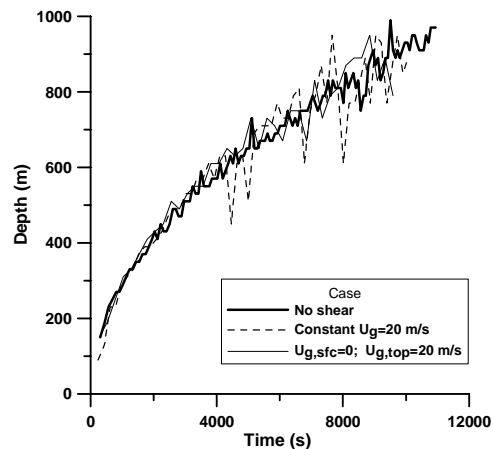


Figure 3. Boundary layer depth versus time using the minimum in buoyancy flux as the definition of CBL top.

In the G20 case, the entrainment rate is significantly reduced in the early part of the simulation but catches up to the other cases fairly quickly after 500 s into the simulation. This slower growth appears to be a result of the developing thermals becoming “smoothed out” by the shear at the surface, decreasing the horizontal temperature variability in the early CBL, thereby reducing the buoyancy forcing term in the linearized, filtered equations of motion. Such retarded entrainment provides some evidence of shear sheltering discussed by Hunt and Durbin (1999). Beyond 1000 s, the differences among the CBL depths are less than their

variability; there is no significant difference in the growth rate.

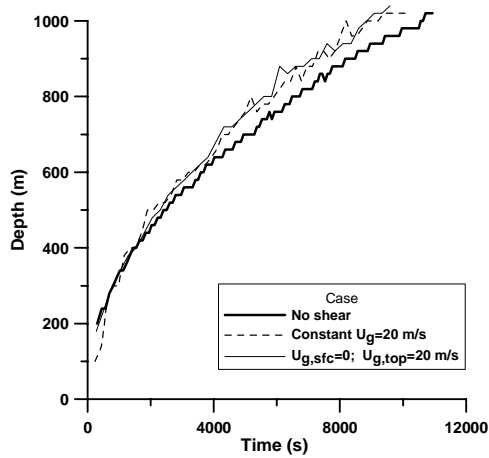


Figure 4. Boundary layer depth versus time using the maximum vertical virtual potential temperature gradient as the definition of CBL top.

The results are different if an alternative definition of CBL depth is used. Figure 4 shows the CBL depth as a function of time using the maximum virtual potential temperature gradient as the definition of the boundary layer top. Using this alternative definition, entrainment is enhanced in both of the cases with shear. Except for the slower initiation of convection in the G20 case, the cases with shear have roughly equal entrainment. These results indicate that the main differences between shear-free and sheared CBL growth may lie within the entrainment zone.

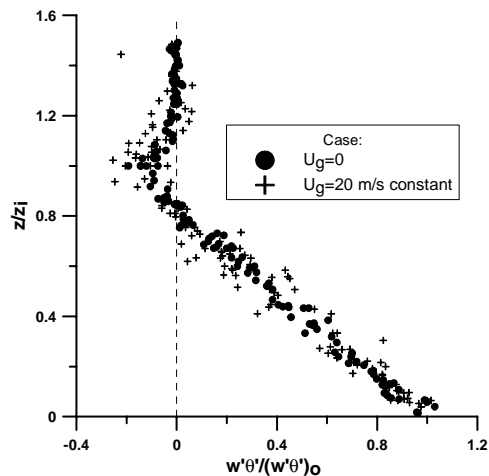


Figure 5. Normalized heat flux profiles for sheared and shear-free cases.

Cases with reduced stratification (not shown) reveal similar results. The effects of shear on CBL growth rate, despite the weaker stratification, appear no different in the simulations with weaker stratification. In fact, the

effects on the level of maximum temperature gradient appear less pronounced.

4.3 Higher order statistics

Figure 5 shows the heat flux profiles normalized to the boundary layer depth, z_i , and the surface heat flux $(w'\theta')_0$. Greater variability in the profile of heat flux is evident in the sheared case. In addition, the modulus of the minimum in heat flux is generally greater with shear than without.

Figure 6 shows the profile of skewness in vertical velocity 6600 s into the shear-free (NS) and constant geostrophic wind (G20) runs. Profiles of heat flux are also shown for convenience as indicators of CBL depth (minimum in heat flux) and the entrainment zone thickness. Here, the entrainment zone is defined as the region between the zero crossing height of the heat flux and the height at which the heat flux once again approaches zero. These skewness profiles are representative of the differences between the two cases at other times as well. The most remarkable difference in skewness is in the entrainment zone. Skewness in the entrainment zone, in the presence of shear, decreases much more rapidly than in the absence of shear, and it also becomes negative. This is a remarkable testimony to the effect of wind shear on thermals within the entrainment zone. Instead of relatively narrow updrafts punching into the inversion as in the shear-free case, updrafts are smoothed by shear as they enter the entrainment zone.

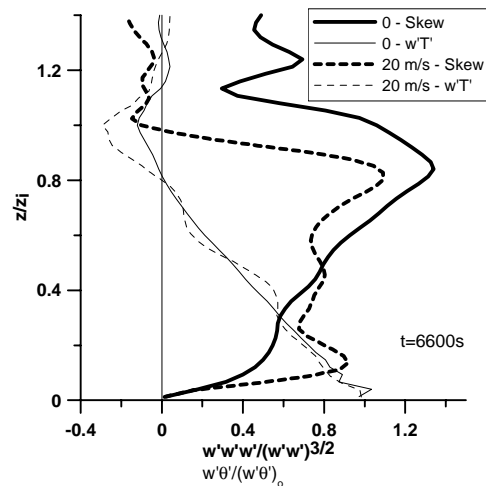


Figure 6. Profiles for vertical velocity skewness at roughly 6600 seconds into the simulation.

Differences also exist near the surface, with some increased skewness in the case with shear (less pronounced in profiles taken at other times), reflecting some organization by updrafts to overcome the effects of strong shear in the surface layer. Elsewhere, skewness is rather similar and reaches a maximum in the lower portion of the entrainment zone.

4.4 Heat flux of entrainment

Shear also appears to have an effect on the heat flux of entrainment. Figure 7 shows the ratio of the heat flux of entrainment to the surface heat flux (C_1) for the three basic cases modeled.

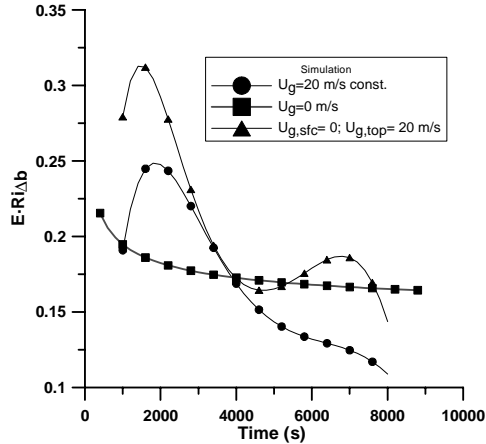


Figure 7. Entrainment ratio as a function of time for the three basic cases.

As reported in Fedorovich and Conzemius (2001), C_1 approaches a value of 0.17 in shear-free cases, but it is much more irregular in cases with wind shear. In the initial stages of the model runs with shear, C_1 appears to grow fairly quickly, reaching a maximum in the early stages of the run. Thereafter, it decreases rapidly and drops below the value for shear-free runs. Although the analysis is somewhat preliminary, the entrainment ratio does change in a manner consistent with CBL growth: slow in the initial stages of the run (small heat flux of entrainment), then rapid (larger heat flux of entrainment), and finally, CBL growth slows during the middle and latter stages of the simulation (heat flux of entrainment decreases).

5. CONCLUDING REMARKS

Although further work is needed to resolve the early stages of the CBL growth and demonstrate some run-to-run consistency in the evolution of heat flux of entrainment, preliminary results provide further evidence of shear sheltering.

The results of the LES runs, in terms of overall boundary layer growth rate, might seem somewhat surprising since shear-generated turbulence might be expected to enhance mixing and thereby increase the entrainment rate in the presence of geostrophic shear, especially for cases where the relative forcing by buoyancy is smaller. Certainly, the results are sensitive to the definition of boundary layer depth, but the decreased heat flux of entrainment during certain stages of sheared LES runs shows that entrainment, at least occasionally, can be hindered by shear. On the other hand, there are times when buoyancy appears to overcome the effects of shear, and rapid entrainment

occurs. More detailed investigations of entrainment over the course of sheared runs, especially in the early stages, are needed to determine when suppressed or enhanced entrainment might be expected. Certainly, the results of this study will need to be considered in conjunction with relevant atmospheric data.

Fedorovich and Conzemius (2001) found that the entrainment rate shows significant departures from the equilibrium regime when the CBL grows through heterogeneously stratified fluids. Similar departures are noted at times in this study in sheared boundary layers. Further investigations will explore the combined effects of both buoyancy and shear on the dynamics of entrainment.

Acknowledgements. The authors are grateful to Mathieu Pourquie for his essential help in the modification of the employed LES code, and to NSF for the provided funding (grant ATM-0124068).

- Brown, A. R., 1996: Large-eddy simulation and parameterization of the baroclinic boundary layer. *Quart. J. Roy. Met. Soc.*, **122**, 1779-1798.
- Fedorovich, E., 1995: Modeling the atmospheric convective boundary layer within a zero-order jump approach: an extended theoretical framework. *J. Appl. Meteor.*, **34**, 1916-1928.
- Fedorovich, E., F. T. M. Nieuwstadt, and R. Kaiser, 2001a: Numerical and laboratory study of a horizontally evolving convective boundary layer. Part I: transition regimes and development of the mixed layer. *J. Atmos. Sci.*, **58**, 70-86.
- Fedorovich, E., F. T. M. Nieuwstadt, and R. Kaiser, 2001b: Numerical and Laboratory Study of a Horizontally Evolving Convective Boundary Layer. Part II: Effects of Elevated Wind Shear and Surface Roughness. *J. Atmos. Sci.*, **58**, 546-560.
- Fedorovich, E., and R. Conzemius, 2001: Large-eddy simulation of convective entrainment in linearly and discretely stratified fluids. *Direct and Large-Eddy Simulation IV*, B. J. Geurts et al., Eds., Kluwer, 435-442.
- Hunt, J. C. R., and P.A. Durbin, 1999: Perturbed vortical layers and shear sheltering. *Fluid Dyn. Res.*, **24**, 375-404.
- Moeng, C.-H., and P. P. Sullivan, 1994: A comparison of shear- and buoyancy-driven planetary boundary layer flows. *J. Atmos. Sci.*, **51**, 999-1022.
- Nieuwstadt, F. T. M., and Brost, R. A., 1986: The decay of convective turbulence. *J. Atmos. Sci.*, **43**, 532-546.
- Sykes, R. I., and D. S. Henn, 1989: Large-eddy simulation of turbulent sheared convection. *J. Atmos. Sci.*, **46**, 1106-1118.
- Wyngaard, J. C., and R. A. Brost, 1984: Top-down and bottom-up diffusion of a scalar in the convective boundary layer. *J. Atmos. Sci.*, **41**, 102-112.